Aerosol and Air Quality Research, 15: 625–633, 2015

ISSN: 1680-8584 print / 2071-1409 online
doi: 10.4209/aaqr.2014.08.0177

Numerical Simulation of Air Flow inside Acoustic Cyclone Separator

Vladas Vekteris, Vytautas Strishka, Darius Ozarovskis, Vadim Mokshin*

Department of Mechanical Engineering, Vilnius Gediminas Technical University, J. Basanavičiaus str. 28, 03224, Vilnius, Lithuania

ABSTRACT

This paper presents a novel concept of cyclone separator, where sound waves are used to agglomerate fine particles. Sound waves generated by Hartmann acoustic generator are introduced into the secondary (core) air flow of cyclone separator. Results of numerical simulation of air flows inside conventional and acoustic cyclone separators are presented. It is shown that intensive pressure pulsations occur in acoustic generator's reflector. These pulsations generate an acoustic field. It is experimentally established that the average separation efficiency of conventional cyclone separator reaches 87.2% only, while separation efficiency of acoustic cyclone separator is approximately 97.5%. Obtained results show that air flows inside cyclone separator can be investigated numerically.

Keywords: Air flow; Acoustic cyclone separator; Particles; Separation efficiency.

INTRODUCTION

Cyclone separator is a simple dust control device with low manufacturing and operating costs and is easy to maintain (Kuo and Tsai, 2001). Air flow inside cyclone separator is divided into two spiraling flows, with the outer flow swirling toward the bottom (primary air flow), while the core flow (secondary air flow) rises from the bottom and is discharged through the outlet (Hsu *et al.*, 2014). The hard, coarse particles moving in the primary air flow of conventional cyclone separator drop out of the flow due to the action of gravity and centrifugal forces. However, particles smaller than 5 μm remain suspended in the secondary air flow (Kuo and Tsai, 2001) and are released into atmosphere. These fine particles, which are the most dangerous because of their ability to penetrate in lung tissue, are difficult to remove by conventional separation technologies (Gallego-Juarez *et al.*, 1999).

Since the time of discovery of cyclone separators over a century ago, many researchers have contributed to the large volume of work on improving the separation efficiency of cyclones by introducing either improved design and operating variables or by new modifications in the design of the equipment (Akhbarifar *et al.*, 2011). However, in the most cases, the efficiency improvement is marginal, and in some cases is associated with complex structure and additional operating costs (Jo *et al.*, 2000). Departing from standard designs, several research groups have tested the performance of small scale sampling cyclone separators varying different standard geometric ratios, and also introducing new designs, although the application of these designs to large-scale cyclone separators is uncertain (Jo *et al.*, 2000).

The separation efficiency can also be improved by additional treatment of polluted air before or inside the air cleaning device in order to agglomerate particles. It was shown in (Vekteris *et al.*, 2012, 2014) that the separation efficiency of separators sufficiently increases after acoustic treatment of the air flow.

Acoustic agglomeration is a process in which high intensity sound waves produce relative motions of particles suspended in gaseous media (Zhang *et al.*, 2012). These motions cause collisions between particles in which they stick together and form larger structures called agglomerates. Then agglomerates continue to connect with each other and become larger and heavier. Usually the sound pressure level of 140–160 dB is used to acoustically agglomerate particles with size less than 1–5 μm (Chernov, 2004; Liu *et al.*, 2009).

Within a short period of time (about 1 s) due to the action of acoustic energy, particles increase in size and become large enough to be caught by traditional air cleaning equipment (Hoffmann, 2000; de Sarabia *et al.*, 2003). Acoustic agglomeration method has indisputable advantages compared to other particle agglomeration techniques (Rosenberg, 1969), for instance, electrostatic precipitation (Parker, 1997).

Acoustic agglomeration process has been widely studied (Mednikov, 1965; Dianov *et al.*, 1968; Rosenberg, 1969; Dong *et al.*, 2006; Sheng and Shen, 2007), but the

* Corresponding author.
Tel.: +370 5 2370594; Fax: +370 5 2700112
E-mail address: vadim.moksin@vgtu.lt

development of this process toward industrial application has been slow. This is caused by the lack of suitable high intensity, high efficiency powerful sound sources and the corresponding full scale agglomeration equipment (Gallego-Juarez *et al.*, 1999). Other researchers report that the influences of the main parameters, especially acoustic frequency, are still not very clear (Liu *et al.*, 2009).

Currently, very few designs of cyclone separators equipped with acoustic air treatment equipment are known. First, special cyclone separator with separate acoustic column should be mentioned (Kochetov *et al.*, 2006). Such system is bulky and requires special maintenance. In addition, the acoustic column does not ensure complex motion of polluted air and acoustic field is used inefficiently. Next, cyclone separator with integrated ultrasonic generator (Khmeliov *et al.*, 2009) can be used to acoustically agglomerate particles and separate them from air. However, such system has limited industrial application, because it is difficult to apply ultrasonic field in large ventilation system ducts. In addition, the ultrasonic source control systems are complex (Hamakawa *et al.*, 2011).

In order to agglomerate fine particles, acoustic cyclone separator with countercurrent air flow (Ozarovskis *et al.*, 2012) was developed. The novelty of this cyclone is that sound waves are introduced into the secondary air flow (rising from the bottom) of the separator. This aim was achieved by placing the Hartmann acoustic generator inside the conical part of the cyclone separator, at the narrowest place. The special air twister was attached above the reflector of the acoustic generator; its inclined blades twist the air reflected from the reflector and direct it in direction opposite to the primary air flow. Thus the secondary air flow effect is enhanced and air supplied to the generator is utilized.

It is very important to study air flow inside acoustic cyclone separator. Additional movements of the air inside cyclone separator can lead to escape of particles from separator. Besides that, these movements can influence the number of collisions between particles. Using numerical simulation techniques can simplify investigations, thus avoiding costly and time-consuming laboratory experiments.

In this study, we suggested a novel concept of cyclone, designed the tangential-flow acoustic cyclone separator, and investigated its air flow using computational fluid dynamics (CFD) method. The novel cyclone separator was analyzed also in terms of particle separation efficiency.

RESEARCH OBJECT

Acoustic cyclone separator presented in Fig. 1 was chosen as the research object. Polluted air (primary air flow 5) is supplied into the cylindrical part 9 of cyclone separator through the inlet 8. Hartmann acoustic generator 3 is located at the bottom of the conical part 6 of cyclone separator. Compressed air is blown into the generator through the pipe 2. Once the air reaches the acoustic generator's reflector 15 (look also at Fig. 2), air pressure pulsations start to occur. Pressure pulsations generate sound waves. Pulsating air exits from generator through the twister's 11 inclined air whirling blades (look also at Fig. 2) and then rises up rotating in the direction opposite to the primary air flow. This countercurrent air flow is mixed with air reflected from the bottom of cyclone separator and rising to the top of the separator (secondary (core) air flow 10). Thus, separating effect of secondary air flow is enhanced.

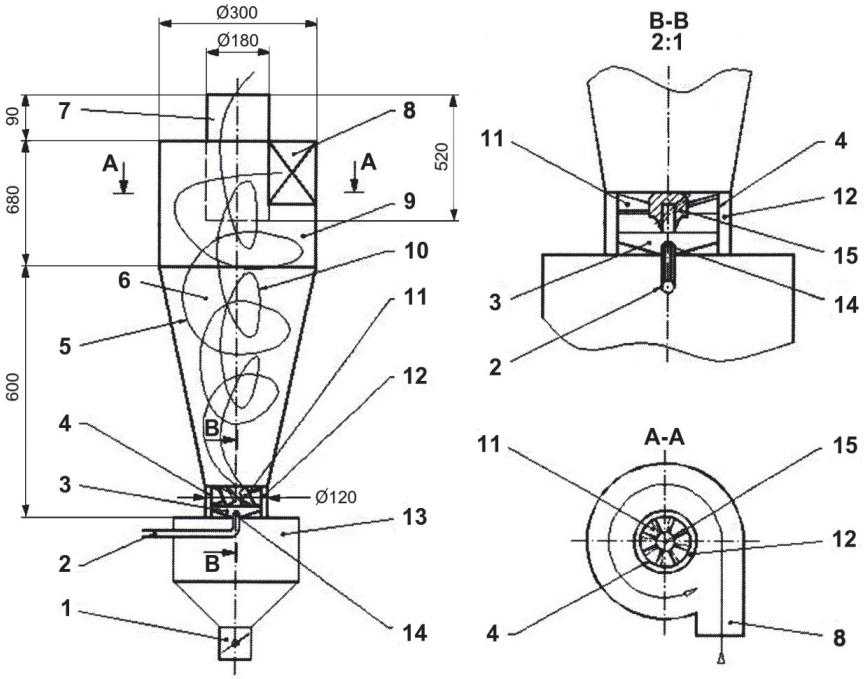

Fig. 1. Acoustic cyclone separator: 1 – gate; 2 – compressed air pipe; 3 – Hartmann acoustic generator; 4 – bushing; 5 – primary air flow; 6 – conical part; 7 – outlet; 8 – inlet; 9 – cylindrical part; 10 – secondary air flow; 11 – twister; 12 – gap; 13 – dust bin; 14 – nozzle; 15 – reflector.

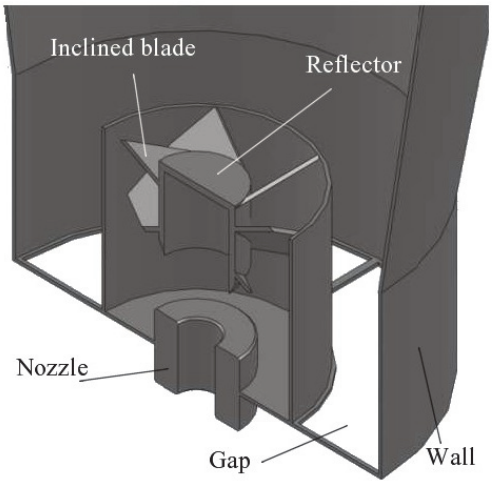

Fig. 2. Section view of acoustic generator.

Frequency of the acoustic excitation can be changed by varying the flow rate of air supplied to the generator. Acoustic cyclone separator can be used also as conventional cyclone separator. In such case no air is supplied to the acoustic generator. Reflector of the acoustic generator is closed by special plug.

Separated particles are collected in the dust bin 13 (Fig. 1). They fall to the collector through the gap 12 between acoustic generator's bushing 4 and cyclone wall.

MATHEMATICAL STUDY

Numerical simulation of air flow inside cyclone separator was performed by solving the Navier-Stokes equations, which are formulations of mass, momentum and energy conservation laws for fluid flows. To predict turbulent flow, the Favre-averaged Navier-Stokes equations were used, where time-averaged effects of the flow turbulence on the flow parameters were considered, whereas the other, i.e., large-scale, time-dependent phenomena were taken into account directly. Through this procedure, extra terms known as the Reynolds stresses appear in the equations. To close this system of equations, transport equations for the turbulent kinetic energy and its dissipation rate were employed (so-called *k-ε* model (Dassault Systemes SolidWorks Corp., 2009)).

The conservation laws for mass, angular momentum and energy in the Cartesian coordinate system rotating with angular velocity Ω about an axis passing through the coordinate system's origin can be written in the conservation form as follows (Dassault Systemes SolidWorks Corp., 2009; Islam and Rakibul Hassan, 2013):

$$\frac{\partial \rho}{\partial t}+\frac{\partial}{\partial x_i}\left(\rho u_i\right)=0 \tag{1}$$

$$\frac{\partial \rho u_i}{\partial t}+\frac{\partial}{\partial x_j}\left(\rho u_i u_j\right)+\frac{\partial p}{\partial x_i}=\frac{\partial}{\partial x_j}\left(\tau_{ij}+\tau_{ij}^R\right)+S_i, \quad i=1,2,3 \tag{2}$$

$$\frac{\partial \rho H}{\partial t}+\frac{\partial \rho u_i H}{\partial x_i}=\frac{\partial}{\partial x_i}\left(u_j\left(\tau_{ij}+\tau_{ij}^R\right)+q_i\right)+\frac{\partial p}{\partial t}-\tau_{ij}^R\frac{\partial u_i}{\partial x_j}+\rho\varepsilon+S_i u_i+Q_H \tag{3}$$

$$H=h+\frac{u^2}{2} \tag{4}$$

where u is the fluid velocity, p is the pressure, t is the time, ρ is the fluid density, S_i is the mass-distributed external force per unit mass, h is the thermal enthalpy, Q_H is the heat source or sink per unit volume, τ_{ij} is the viscous shear stress tensor, τ_{ij}^R is the Reynolds-stress tensor, q_i is the diffusive heat flux, and ε is the turbulent dissipation. The subscripts are used to denote summation over the three coordinate directions.

Two additional transport equations were used to describe the turbulent kinetic energy and dissipation (Dassault Systemes SolidWorks Corp., 2009):

$$\frac{\partial \rho k}{\partial t}+\frac{\partial}{\partial x_i}\left(\rho u_i k\right)=\frac{\partial}{\partial x_i}\left(\left(\mu+\frac{\mu_t}{\sigma_k}\right)\frac{\partial k}{\partial x_i}\right)+S_k \tag{5}$$

$$\frac{\partial \rho \varepsilon}{\partial t}+\frac{\partial}{\partial x_i}\left(\rho u_i \varepsilon\right)=\frac{\partial}{\partial x_i}\left(\left(\mu+\frac{\mu_t}{\sigma_\varepsilon}\right)\frac{\partial \varepsilon}{\partial x_i}\right)+S_\varepsilon \tag{6}$$

where σ_k, σ_ε are the constants, μ is the dynamic viscosity coefficient, μ_t is the turbulent eddy viscosity coefficient, k is the turbulent kinetic energy, and S_k and S_ε are the source terms.

If the Lewis number Le = 1 the diffusive heat flux is defined as (Dassault Systemes SolidWorks Corp., 2009):

$$q_i=\left(\frac{\mu}{\mathrm{Pr}}+\frac{\mu_t}{\sigma_c}\right)\frac{\partial h}{\partial x_i}, \quad i=1,2,3 \tag{7}$$

where Pr is the Prandtl number, and σ_c is the constant (σ_c = 0.9).

The cell-centered finite volume method was used to obtain conservative approximations of the governing equations on the locally refined rectangular mesh. The governing equations are integrated over a control volume which is a grid cell, and then approximated with the cell-centered values of the basic variables. The integral conservation laws may be represented in the form of the cell volume and surface integral equation and written in the discrete form (Dassault Systemes SolidWorks Corp., 2009; Islam and Rakibul Hassan, 2013):

$$\frac{\partial}{\partial t}\left(\mathrm{Uv}\right)+\sum_n \mathrm{Fs}=\mathrm{Qv} \tag{8}$$

where n is the number of cell faces.

The second-order upwind approximations of fluxes F are based on the implicitly treated modified Leonard's QUICK Approximations (Panton, 1996) and the Total Variation Diminishing (TVD) method (White, 1994).

RESULTS AND DISCUSSION

Numerical Simulation of Air Flow inside Conventional Cyclone Separator

Calculation scheme of conventional cyclone separator and its 3D models are presented in Fig. 3. Initial and boundary conditions are presented in Table 1.

It was simulated that quartz sand particles were introduced into the primary air flow of cyclone separator. It was assumed that particles were distributed evenly in the air flow and had spherical shape. Simulation results are presented in Fig. 4 and Table 2.

It can be seen from Table 2 and Figs. 4(a), 4(c) that the difference between minimum and maximum air pressure and temperature values does not exceed 1% and is insignificant.

After analyzing the air velocity map (Fig. 4(b)), we can conclude that the maximum values are observed at the periphery of the primary air flow of cyclone separator. The velocity of the primary air flow near the inner wall of the cylindrical part is about 18 m/s. Air velocity starts to decrease in the conical part of cyclone separator and decreases to zero at the bottom of the conical part. Velocity also significantly decreases in direction of the axis of cyclone separator. The primary air flow disappears near the axis of cyclone separator, but secondary flow (core flow) appears. Its average velocity is about 5 m/s.

It can be seen from Table 2 that the particle velocity component values differ slightly from those of the air flow.

Calculated air velocity values (Fig. 4(b)) are in good concordance with experimentally obtained ones presented in (Vekteris *et al.*, 2014).

Numerical Simulation of Air Flow inside Acoustic Cyclone Separator

In such a case, additional air flow is supplied to the acoustic generator located at the bottom of the conical part of cyclone separator. The boundary conditions of this air flow are presented in Table 3. Other simulation conditions were the same as those presented in Table 1. Calculation scheme of acoustic cyclone separator is presented in Fig. 5.

Simulation results are presented in Figs. 6, 7 and Table 4.

It can be seen from Table 4, Fig. 6(c) and Fig. 7 that minimum and maximum pressure values differ about five times. Such difference appears due the air flow passed through the acoustic generator.

The main peculiarity of acoustic cyclone separator is integrated acoustic generator located at the bottom. As numerical simulations have shown, intensive pressure pulsations occur near its reflector. The pressure varies from 54.4 to 267.6 kPa in the acoustic generator (Fig. 7). Pressure pulsations generate an acoustic field. Air flow trajectories inside the generator also are seen in Fig. 7.

Countercurrent (in respect of the direction of the primary air flow) swirling air flow (secondary or core air flow) is formed in the bottom of acoustic cyclone separator. While rising up the cyclone separator, the countercurrent vortex loses kinetic energy and yields to the primary flow. This process can be seen in Fig. 6(b). It can be also seen from Fig. 6(b) that the secondary air flow does not influence the velocity of the primary air flow near the wall of the cylindrical part of cyclone separator. Air velocity at the periphery of the primary air flow is about 18 m/s, i.e., is the same as in case of conventional cyclone separator. It should also be mentioned that a much larger vortex (core flow) compared with conventional cyclone separator is formed in the bottom of acoustic cyclone separator. Its average velocity is about 8 m/s.

The most complex air flow trajectories are observed in the bottom of acoustic cyclone separator. It can be stated that air flow is chaotic in the conical part of acoustic cyclone

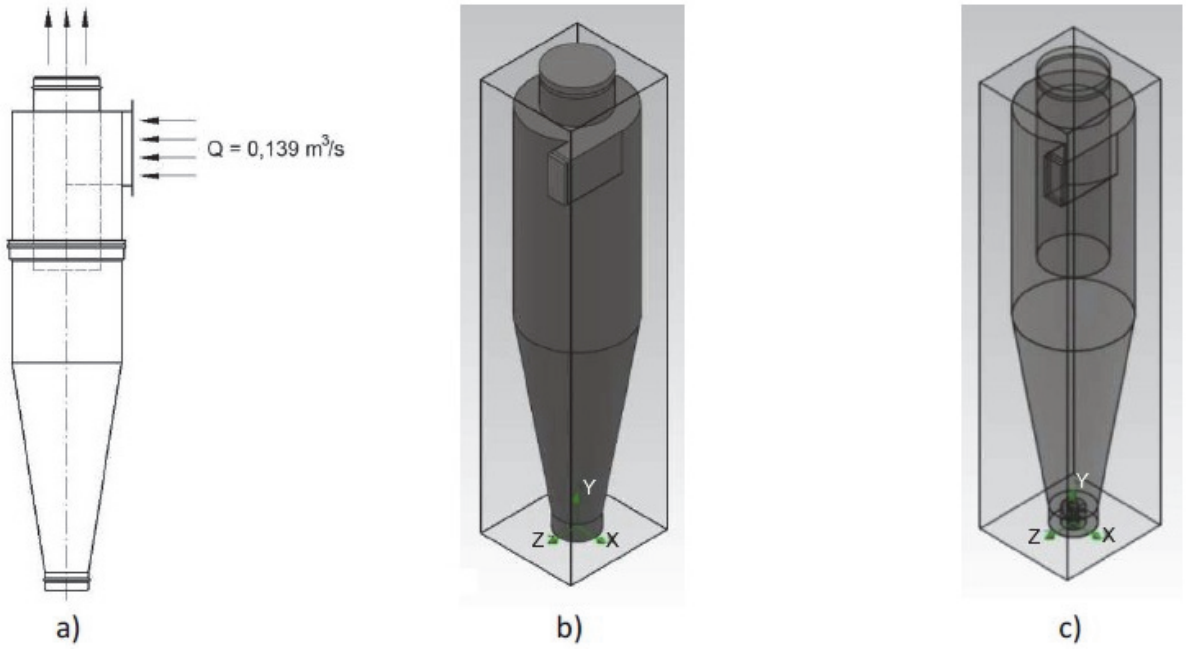

Fig. 3. Conventional cyclone separator: a) – calculation scheme; b) – 3D solid model; c) – 3D transparent model.

Table 1. Initial and boundary conditions (conventional cyclone separator).

Initial conditions	
Thermodynamical parameters	Static pressure 101325 Pa
	Temperature 293.20 K
Velocity parameters	Velocity vector components:
	Velocity in direction of X axis 0 m/s
	Velocity in direction of Y axis 0 m/s
	Velocity in direction of Z axis 0 m/s
Fluid	Air
Boundary conditions of primary air flow	
Surface	Cross-section of the inlet
Parameters of the flow	Flow vector direction: normal to the surface
	Flow rate 0.139 m^3/s
Thermodynamical parameters	Approximate pressure 101325 Pa
	Temperature 293.20 K
Turbulence parameters	Turbulence intensity 2.00%
	Turbulence length 0.003 m
Parameters of the boundary layer	Type: Turbulent
Boundary conditions of outtake air flow	
Surface	Cross-section of the outlet pipe
Parameters of the flow	Flow vector direction: normal to the surface
Coordinate system	Surface coordinate system
Thermodynamical parameters	Environmental air pressure 101325 Pa
	Temperature 293.20 K
Turbulence parameters	Turbulence intensity 2.00%
	Turbulence length 0.003 m
Parameters of the boundary layer	Type: Turbulent
Parameters of the walls	
Roughness	0
Type	Adiabatic (heat-insulated)

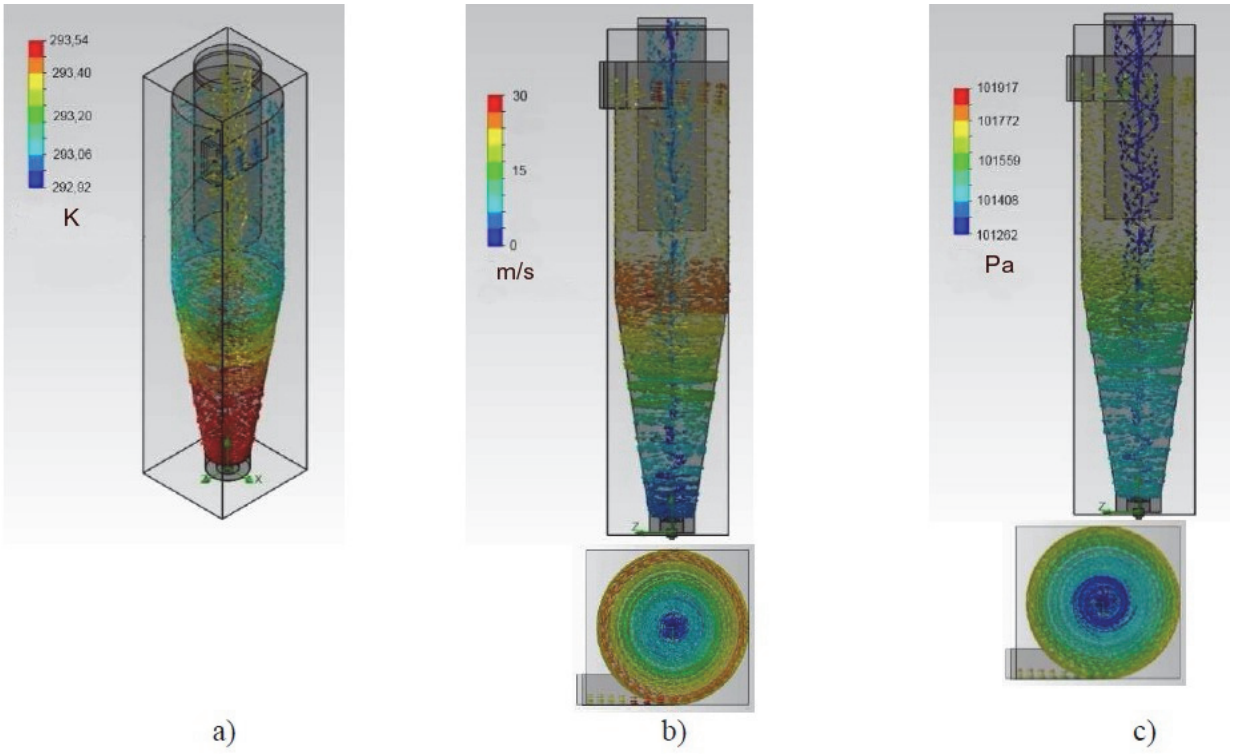

Fig. 4. Results of numerical simulation of air flow inside conventional cyclone separator: a) – temperature; b) – velocity; c) – pressure.

Table 2. Numerical simulation results (conventional cyclone separator).

Name of the parameter	Value	
	Minimum	Maximum
Pressure inside cyclone separator, Pa	101263.70	101837.78
Air temperature, K	292.96	293.60
Velocity of the air, m/s	0	30.106
Velocity component along X axis, m/s	–26.926	23.417
Velocity component along Y axis, m/s	–12.803	11.625
Velocity component along Z axis, m/s	–29.978	25.115
Mach number	0	0.09
Density, kg/m^3	1.20	1.21
Particle velocity, m/s	0.006	23.842
Particle velocity along the X axis, m/s	–23.688	22.535
Particle velocity along the Y axis, m/s	–9.675	11.213
Particle velocity along the Z axis, m/s	–23.176	22.812
Particle density, kg/m^3	2600	2600
Particle temperature, K	293.09	293.59
Reynolds number	0	162.6939921
Particle weight, kg	$1.361 \cdot 10^{-9}$	$1.361 \cdot 10^{-9}$
Particle size, m	$1.00 \cdot 10^{-4}$	$1.00 \cdot 10^{-4}$
Relative velocity of the particle, m/s	0	24.456

Table 3. Boundary conditions of countercurrent air flow (acoustic cyclone separator).

Boundary conditions of countercurrent air flow (secondary)	
Surface	Cross-section of the pipe
Parameters of the flow	Flow vector direction: normal to the surface
	Flow rate 0.005 m^3/s
Thermodynamical parameters	Approximate pressure 101325 Pa
	Temperature 293.20 K
Turbulence parameters	Turbulence intensity 2.00%
	Turbulence length 0.003 m
Parameters of the boundary layer	Type: Turbulent

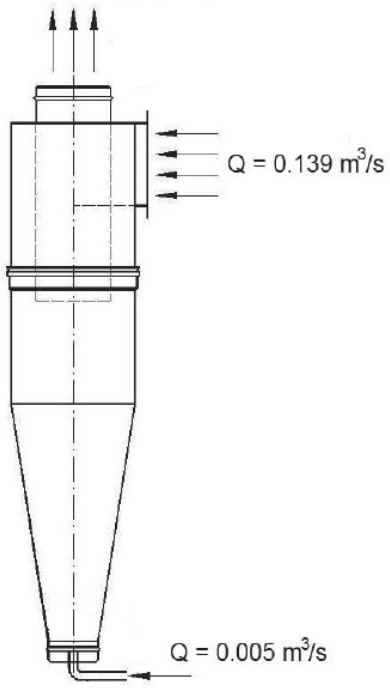

Fig. 5. Calculation scheme of acoustic cyclone separator.

separator. Air velocity reaches 200–400 m/s near the acoustic generator's reflector, the Mach number varies from 0 to 1.34 (Table 4). Temperature of the air in the conical part of cyclone separator rises to 40–80°C (Fig. 6(a), Table 4). Temperature of the particles rises to 80°C as well (Table 4).

Investigation of Separation Efficiency of Acoustic Cyclone Separator

Separation efficiency of conventional and acoustic cyclone separators was evaluated experimentally. A known amount of quartz sand (particle size 0–20 μm, density 2600 kg/m^3, moisture content < 0.5%) was introduced into the primary air flow by means of dispenser. Then separated particles were removed from the dust bin and weighed by precise scale with accuracy of 0.001 g. Separation efficiency of cyclone separator was calculated knowing the exact weight of sand injected into the air and the weight of sand collected in the dust bin.

Experiments with acoustic cyclone separator were carried out at different flow rates of air supplied to the acoustic generator and, as a result, at different acoustic field frequencies. Results are presented in Fig 8.

It can be seen from Fig. 8 that separation efficiency of conventional cyclone separator varies from 85.7% to 88.5%

Table 4. Numerical simulation results (acoustic cyclone separator).

Name of the parameter	Value	
	Minimum	Maximum
Pressure inside cyclone separator, Pa	54411.35	267637.33
Air temperature, K	219.94	355.67
Velocity of the air, m/s	0	432.106
Velocity component along X axis, m/s	–424.132	415.137
Velocity component along Y axis, m/s	–216.889	353.105
Velocity component along Z axis, m/s	–412.911	415.963
Mach number	0	1.34
Density, kg/m^3	0.66	2.68
Particle velocity, m/s	2.780	58.494
Particle velocity along the X axis, m/s	–42.720	31.343
Particle velocity along the Y axis, m/s	–7.811	48.503
Particle velocity along the Z axis, m/s	–31.905	32.324
Particle density, kg/m^3	2600	2600
Particle temperature, K	293.09	354.36
Reynolds number	0	230.6413642
Particle weight, kg	$1.361 \cdot 10^{-9}$	$1.361 \cdot 10^{-9}$
Particle size, m	$1.00 \cdot 10^{-4}$	$1.00 \cdot 10^{-4}$
Relative velocity of the particle, m/s	0	48.518

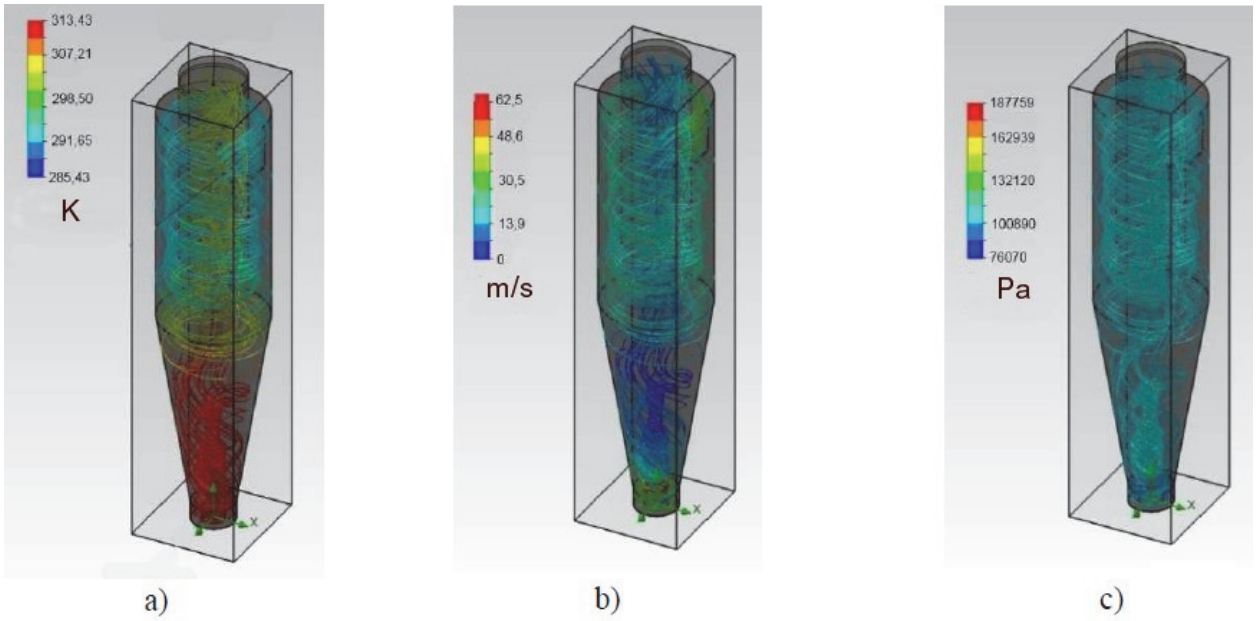

Fig. 6. Results of numerical simulation of air flow inside acoustic cyclone separator: a) – temperature; b) – velocity; c) – pressure.

(average 87.2%) while separation efficiency of acoustic cyclone separator varies from 97.1% to 98.0% (average 97.5%). Therefore, it can be stated that the secondary air flow and acoustic field have a positive effect on separation efficiency of cyclone separator. The greatest separation efficiency of acoustic cyclone separator was obtained at acoustic field frequency of 8 kHz.

The ratio of particle number concentration after the sound application to that before the sound application, n/n_0, was used to compare the effectiveness of acoustic agglomeration of fine particles of different sizes. The values of n/n_0 measured by means of "Lasair II" particle counter are shown in Fig. 9. After acoustic agglomeration in acoustic cyclone separator, the concentration of particles in air decreased dramatically. It can be seen in Fig. 9 that the concentration of finer particles changes less than the concentration of coarser particles. The number concentration of 0.3 μm particles was reduced by 53.5% only. However, 73.1% of 0.5 μm particles were removed by acoustic cyclone separator. Finally, the number concentration of 1 μm particles was reduced by 94%.

CONCLUSIONS

1. Presence of countercurrent air flow has significant

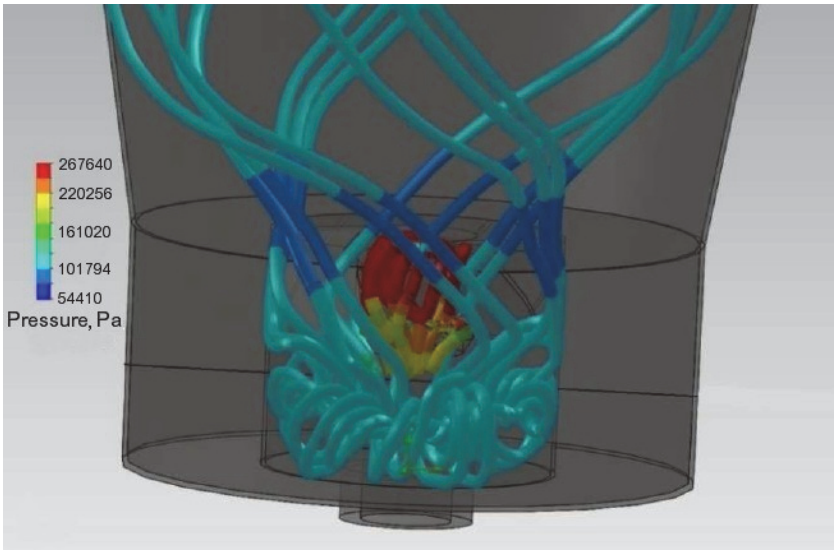

Fig. 7. Pressure pulsations inside the acoustic generator.

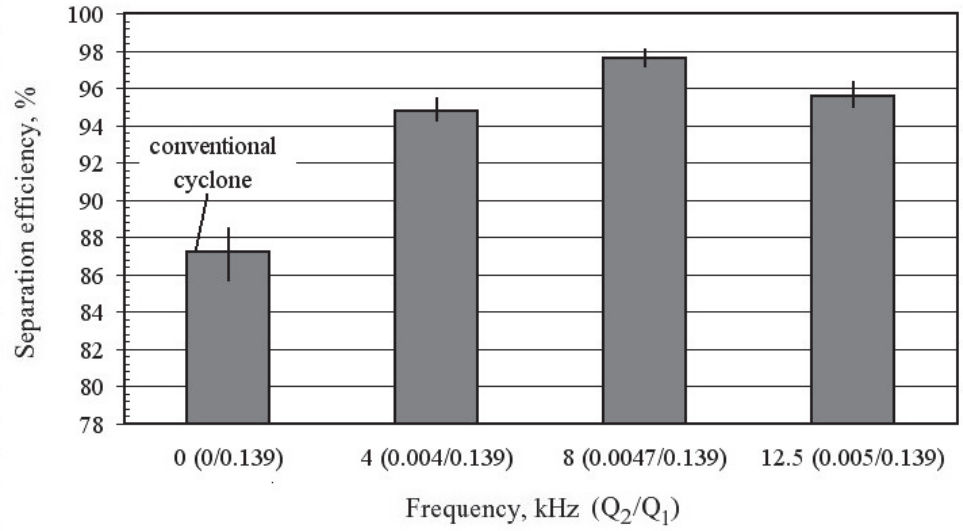

Fig. 8. Average separation efficiency of cyclone separator versus acoustic field frequency and ratio Q_2/Q_1: Q_1 is the flow rate of the primary air flow, m^3/s; Q_2 is the flow rate of the air flow supplied to the acoustic generator, m^3/s.

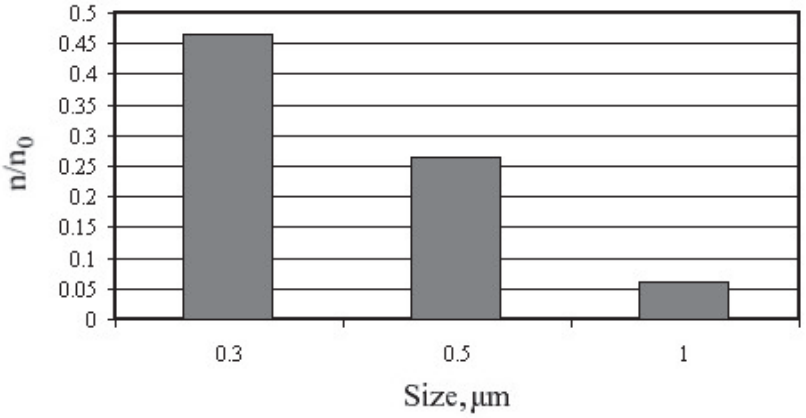

Fig. 9. The ratio n/n_0 as function of particle size: n_0 is the number of particles in 1 m^3 of air before the sound application; n is the number of particles in 1 m^3 of air after the sound application (sound pressure level of 130–170 dB, acoustic field frequency of 8 kHz).

influence on following characteristics of air flow inside acoustic cyclone separator: trajectory, velocity, pressure, temperature and velocity of the particles.

2. Numerical simulation shows that the largest pressure changes occur in the acoustic generator. Minimum pressure reaches 54.4 kPa, maximum – 267.6 kPa. Pressure pulsations generate sound waves which act on particles. Particles stick together; their agglomerates become larger and heavier and then are removed from air flow due to the action of gravitational and centrifugal forces.
3. The average separation efficiency of conventional cyclone separator reaches 87.2% while separation efficiency of acoustic cyclone separator – 97.5%.
4. The highest separation efficiency of acoustic cyclone separator is achieved when polluted air flow is affected by acoustic field of 8 kHz frequency.
5. Obtained results show that air flow inside cyclone separator can be investigated numerically, thus avoiding costly and time-consuming experiments.

REFERENCES

Akhbarifar, S., Shirvani, M., Zahedi, S., Zahiri, M.R. and Shamsaii, Y. (2011). Improving Cyclone Efficiency by Recycle and Jet Impingement Streams. *Iran. J. Chem. Chem. Eng.* 30: 119–124.

Chernov, N.N. (2004). Acoustic Methods and Means of Precipitation of Particles of Industrial Smokes, Ph. D. Thesis, Taganrog State Radioengineering University.

Dassault Systemes SolidWorks Corp. (2009). *SolidWorks Flow Simulation 2009 Technical Reference*, Waltham.

de Sarabia, E.R.F., Elvira-Segura, L., Gonzalez-Gomez, I., Rodriguez-Maroto, J.J., Munoz-Bueno, R. and Dorronsoro-Areal, J.L. (2003). Investigation of the Influence of Humidity on the Ultrasonic Agglomeration of Submicron Particles in Diesel Exhausts. *Ultrasonics* 41: 277–281.

Dianov, D.B., Podolskii, A.A. and Turubarov, V.I. (1968). Calculation of the Hydrodynamic Interaction of Aerosol Particles in a Sound Field under Oseen Flow Conditions. *Sov. Phys. Acoust.* 13: 314–319.

Dong, S., Lipkens, B. and Cameron, T.M. (2006). The Effects of Orthokinetic Collision, Acoustic Wake, and Gravity on Acoustic Agglomeration of Polydisperse Aerosols. *J. Aerosol Sci.* 37: 540–553.

Gallego-Juarez, J.A., de Sarabia, E.R.F., Rodriguez-Corral, G., Hoffmann, T.L., Galvez-Moraleda, J.C., Rodriguez-Maroto, J.J., Gomez-Moreno, F.J., Bahillo-Ruiz, A., Martin-Espigares, M. and Acha, M. (1999). Application of Acoustic Agglomeration to Reduce Fine Particle Emissions from Coal Combustion Plants. *Environ. Sci. Technol.* 33: 3843–3849.

Hamakawa, H., Arshad, A.B.M. and Ohta, M. (2011). Effect of Acoustic Resonance Phenomenon on Fluid Flow with Light Dust. *J. Therm. Sci.* 20: 430–434.

Hoffmann, T.L. (2000). Environmental Implications of Acoustic Aerosol Agglomeration. *Ultrasonics* 38: 353–357.

Hsu, C.W., Huang, S.H., Lin, C.W., Hsiao, T.C., Lin, W.Y. and Chen, C.C. (2014). An Experimental Study on Performance Improvement of the Stairmand Cyclone Design. *Aerosol Air Qual. Res.* 14: 1003–1016.

Islam, T. and Rakibul Hassan, S.M. (2013). Experimental and Numerical Investigation of Flow over a Cylinder at Reynolds Number 10^5. *J. Mod. Sci. Technol.* 1: 52–60.

Jo, Y., Tien, C. and Ray, M.B. (2000). Development of a Post Cyclone to Improve the Efficiency of Reverse Flow Cyclones. *Powder Technol.* 113: 97–108.

Khmeliov, V.N., Shalunov, A.V., Tsyganok, S.N. and Shalunova, K.V. (2009). Use of High Intensity Ultrasonic Vibrations to Increase Efficiency of Gas Cleaning Equipment, Proc. of Int. Conf. Gas Cleaning 2009, Moscow, Russia, p. 96–100.

Kochetov, O.S., Kochetova, M.O. and Hodakova, T.D. (2006). Acoustic Cyclone, RU Patent RU2268090.

Kuo, K.Y. and Tsai, C.J. (2001). On the Theory of Particle Cutoff Diameter and Collection Efficiency of Cyclones. *Aerosol Air Qual. Res.* 1: 47–56.

Liu, J., Zhang, G., Zhou, J., Wang, J., Zhao, W. and Cen, K. (2009). Experimental Study of Acoustic Agglomeration of Coal-Fired Fly Ash Particles at Low Frequencies. *Powder Technol.* 193: 20–25.

Mednikov, E.P. (1965). *Acoustic Coagulation and Precipitation of Aerosols*, Consultants Bureau, New York.

Ozarovskis, D., Vekteris, V. and Striška, V. (2012). Acoustic Cyclone, LT Patent LT5846 (B).

Panton, R.L. (1996). *Incompressible Flow*, John Wiley & Sons, Inc., New York.

Parker, K.R. (Ed.) (1997). *Applied Electrostatic Precipitation*, Blackie Academic & Professional, London.

Rosenberg, L.D. (1969). *Physical Basis of Ultrasound Technologies*, Science, Moscow.

Sheng, C. and Shen, X. (2007). Simulation of Acoustic Agglomeration Processes of Poly-Disperse Solid Particles. *Aerosol Sci. Technol.* 41: 1–13.

Vekteris, V., Striška, V., Ozarovskis, D. and Mokšin, V. (2012). Tribological Adhesion of Particles in Acoustic Field. *J. Vibroeng.* 14: 509–513.

Vekteris, V., Strishka, V., Ozarovskis, D. and Mokshin, V. (2014). Experimental Investigation of Processes in Acoustic Cyclone Separator. *Adv. Powder Technol.* 25: 1118–1123

White, F.M. (1994). *Fluid Mechanics*, McGraw-Hill, New York.

Zhang, G., Liu, J., Wang, J., Zhou, J. and Cen, K. (2012). Numerical Simulation of Acoustic Wake Effect in Acoustic Agglomeration under Oseen Flow Condition. *Chin. Sci. Bull.* 57: 2404–2412.

Received for review, August 25, 2014
Revised, November 9, 2014
Accepted, November 15, 2014